ACS APPLIED MATERIALS & INTERFACES

Research Article

www.acsami.org

An 8.68% Efficiency Chemically-Doped-Free Graphene–Silicon Solar Cell Using Silver Nanowires Network Buried Contacts

Lifei Yang, Xuegong Yu,* Weidan Hu, Xiaolei Wu, Yan Zhao, and Deren Yang*

State Key Lab of Silicon Materials and Department of Materials Science and Engineering, Zhejiang University, Hangzhou 310027, P.R. China

Supporting Information

ABSTRACT: Graphene–silicon (Gr-Si) heterojunction solar cells have been recognized as one of the most low-cost candidates in photovoltaics due to its simple fabrication process. However, the high sheet resistance of chemical vapor deposited (CVD) Gr films is still the most important limiting factor for the improvement of the power conversion efficiency of Gr-Si solar cells, especially in the case of large device-active area. In this work, we have fabricated a novel transparent conductive film by hybriding a monolayer Gr film with silver nanowires (AgNWs) network soldered by the graphene oxide (GO) flakes. This Gr-AgNWs hybrid film exhibits low sheet resistance and larger direct-current to optical conductivity ratio, quite suitable for solar cell fabrication. An efficiency of 8.68% has been achieved for the Gr-AgNWs-Si solar cell, in which the AgNWs network acts as buried contacts. Meanwhile, the Gr-AgNWs-Si solar cells have much better stability than the chemically doped Gr-Si solar cells. These results show a new route for the fabrication of high efficient and stable Gr-Si solar cells.

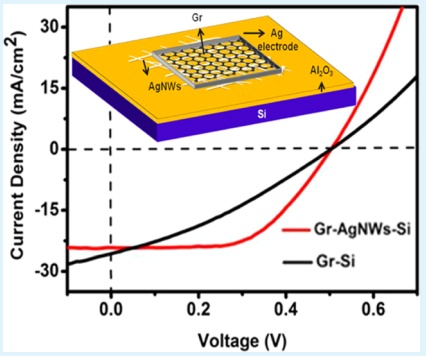

KEYWORDS: *graphene, silicon, solar cell, silver nanowire, buried contact*

INTRODUCTION

Graphene (Gr), as a novel type of two-dimensional materials, has fascinating properties, including ultra-high carrier mobility and transparency,[1] which can be grown by chemical vapor deposition (CVD).[2] Therefore, there is growing interest in combining graphene (Gr) with silicon (Si) to develop photovoltaic (PV) devices.[3] The fabrication of Gr-Si solar cells can usually be accomplished by simply transferring Gr films onto Si substrates at room temperature, which is considered as one of the most low-cost candidates in PV application, due to the absence of p–n junction. In Gr-Si solar cells, the Gr film not only can allow light transmission into Si substrate but also can form interface junction with Si for the separation of electron–hole pairs.[4] The first Gr-Si solar cell fabricated by Li et al.[5] in 2010 achieved an efficiency of 1.5%. Subsequently, many strategies have been applied to improve the efficiency of the Gr-Si solar cell, such as enhancing light absorption by using Si nanoarray[6] and suppressing Gr-Si interface recombination by using a poly(3-hexylthiophene) (P_3HT)[7] or graphene oxide (GO) interlayer, which helps improve the efficiency of the pristine monolayer Gr–Si solar cell to 6.18%.[8] However, such an efficiency of Gr-Si solar cells is still much lower than that of crystalline Si solar cells based on p–n junction.

Generally, the optoelectronic properties of Gr films, including its transparence and sheet resistance, are very critical for the performance improvement of Gr/Si solar cells.[9] Even though the optical transparency of monolayer Gr films is about 97.7%,[10] the sheet resistance of CVD-grown polycrystalline Gr films is usually in the range 125–1000 Ω/□,[11] much higher than that of Si emitters (40–60 Ω/□) in commercial crystalline Si solar cells. Such a high sheet resistance of Gr films cannot meet the requirement of high efficiency solar cells. Thus, various methods have been explored to improve the electrical conductivity of Gr films. Chemical doping is usually utilized to reduce the sheet resistance of Gr films and therefore improve the efficiency of Gr-Si solar cells. A maximum efficiency of 8.6% has already been reported for the monolayer Gr-Si solar cell though doping the Gr film by bis-(trifluoromethanesulfonyl) amide [$(CF_3SO_2)_2NH$] (TFSA).[12] However, it is noticed that the sheet resistance of the chemically doped monolayer Gr film is still not sufficiently low enough to reduce resistance-induced power loss of the Gr-Si solar cell, especially in the case of large device-active area. For example, it was reported when the device-active area was scaled up from 4.7 mm^2 to 14.5 mm^2, the fill factor of chemically doped Gr-Si solar cells decreased from 72% to 50%, due to the resistance loss of the solar cell.[13] Moreover, the chemically doped Gr film was generally not stable, which resulted in a severe efficiency degradation for solar cells in few days, not suitable for practical application.[14]

In this work, we have tried to hybrid the Gr film with a silver nanowires (AgNWs) network. The AgNWs network is soldered using graphene oxide (GO) flakes, which exhibits excellent

Received: November 22, 2014
Accepted: February 2, 2015
Published: February 2, 2015

DOI: 10.1021/am508211e
ACS Appl. Mater. Interfaces 2015, 7, 4135–4141

thermal stability, and conductivity. The sheet resistance of the Gr-AgNWs hybrid films can be reduced down to 9Ω/□ and keeps the transparency as high as 78% (at the wavelength of 550 nm). An efficiency of 8.68% can be obtained for the Gr-AgNWs-Si solar cell with a device-active area of 16 mm^2. Moreover, it is clarified that such Gr-AgNWs-Si solar cell shows better stability than the chemically doped Gr-Si solar cells, more suitable for practical application.

EXPERIMENTAL DETAILS

Raw Materials. AgNWs with average diameters of 90 nm and lengths of 20 μm in isopropyl alcohol (IPA) (10 mg/mL) were purchased from Blue Nano. Single layer GO powder with average flake size of 1 um and thickness of 0.8 nm was obtained from XFNANO. The monolayer Gr film was produced by a copper (Cu) catalyzed low pressure CVD (LPCVD) method at 1000 °C, using CH_4 (20 sccm) as the carbon source and H_2 (40 sccm) as the reduction gas. The AgNWs ink (0.5 mg/mL) was obtained by diluting the AgNWs dispersion with IPA. The GO solution (0.5 mg/mL) was prepared by dispersing the GO powder in a mixed solvent of deionization water and IPA (1:1, volume ratio).

Preparation and Characterization of Gr-AgNWs Hybrid Film. After being stirred for 10 min using a magnetic stir bar, the AgNWs ink was spin coated on a precleaned glass substrate to form AgNWs network. The spin rate and time were 1000 rpm and 30 s, respectively. The AgNWs density in the network is modified by controlling the spin coating cycles (2, 3, 5, 7 cycles). The formed AgNWs network was heated at 100 °C for 2 min to evaporate the solvent and then soaked in the GO solution for 5 min, followed by distilled water rinsing and N_2 flow drying. Subsequently, a monolayer Gr with sheet resistance of 400−1000 Ω/□ was transferred onto the AgNWs network to form a Gr-AgNWs hybrid film using the traditional Poly(methyl methacrylate) (PMMA) assisted wet transfer process.[15] The sheet resistances of the AgNWs networks and the Gr-AgNWs hybrid films were measured with a Hall system (Lakeshore) and the transmittances were studied by a UV−vis absorption spectrometer (Varian Cary 100).

Fabrication and Performance Evaluation of Gr-AgNWs-Si Solar Cells. N-type ⟨100⟩ Czochralski (CZ) Si wafer with resistivity of 1−3 Ω·cm was used as a substrate for the device fabrication. An ultrathin (1.9 nm) Al_2O_3 film was deposited on the Si substrate for surface passivation by atomic layer deposition (ALD) technology. The AgNWs-Gr hybrid film was then formed on the Si substrate following the approach described above (see Supporting Information Figure S1). Subsequently, a 400 °C/60 min annealing in forming gas is used to optimize the contact of the Gr film on Si. Finally, the Ag paste was applied around the Gr to enclose a nearly square window as the device-active area for the solar cells and the back contact was made by scratching the InGa eutectic alloy at the Si backside. Some reference Gr-Si solar cells without AgNWs network buried contacts and some reference AgNWs-Si devices without top Gr film were fabricated by the similar process. The performances of solar cells were measured using a Keithley 2400 source meter and a solar simulator under AM 1.5G condition at an illumination intensity of 100 mW/cm^2, calibrated by a standard Si solar cell.

RESULTS AND DISCUSSION

Figure 1 shows the SEM and AFM images of AgNWs network soldered by GO flakes. It can be seen that the GO flakes are selectively wrapped around the junctions of the AgNWs, which is same to the experimental results reported by Liang et al.[16] Figure 2a shows the SEM image of Gr-AgNWs hybrid film. It can be seen that the Gr film forms corrugation along the AgNWs. By comparing the AFM images of AgNWs network soldered by GO flakes (Figure 1b, c) and that of Gr-AgNWs hybrid film (Figure 2b, c), it can be found that the Gr film covers the AgNWs network very well. Figure 3a shows the sheet resistances of AgNWs networks, AgNWs networks soldered by GO flakes and Gr-AgNWs hybrid films as a function of AgNWs density. The AgNWs density can be

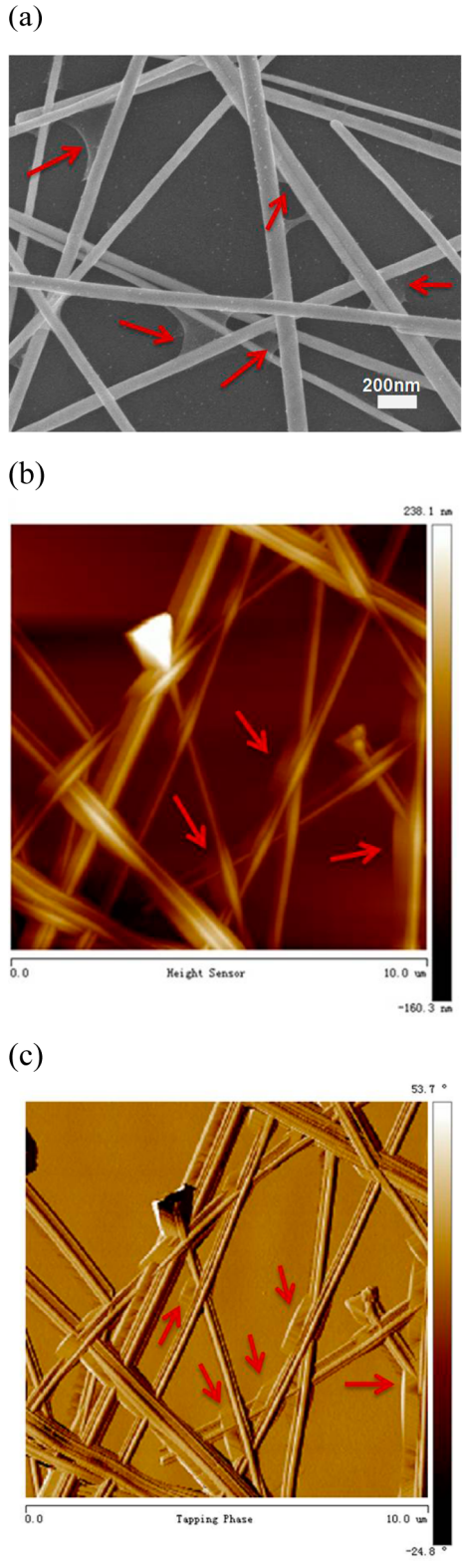

Figure 1. (a) SEM image of GO soldered AgNWs Network. The arrows show the location of GO flakes. (b) AFM image of GO soldered AgNWs Network in height contrast mode. The arrows show the locations of the GO flakes. (c) AFM image of GO soldered AgNWs Network in phase contrast mode. The arrows show the locations of the GO flakes.

DOI: 10.1021/am508211e
ACS Appl. Mater. Interfaces 2015, 7, 4135−4141

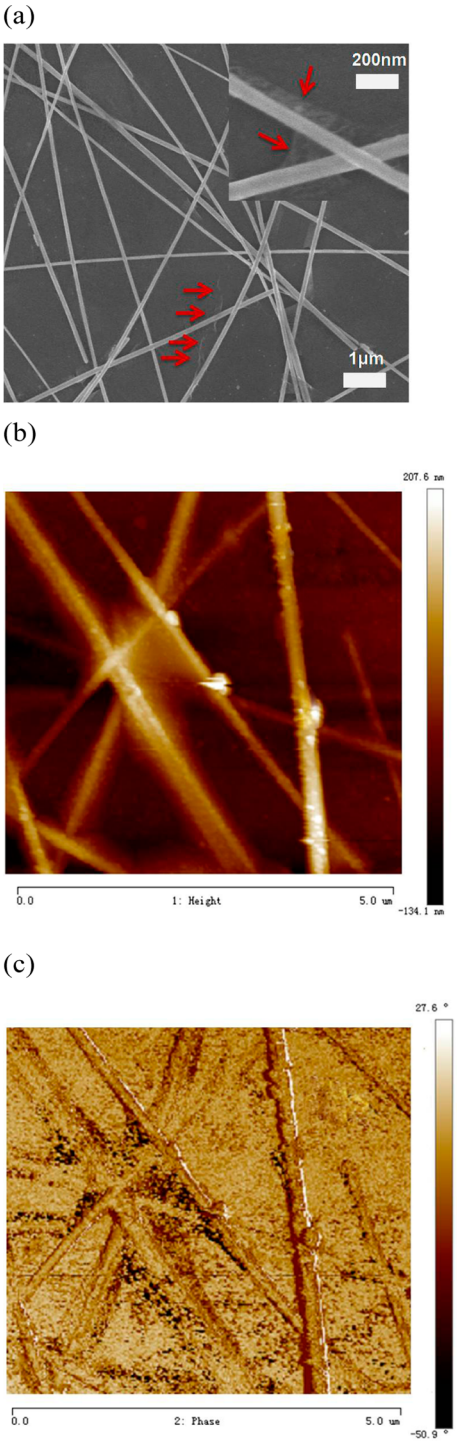

Figure 2. (a) SEM image of Gr-AgNWs hybrid film. The arrows show the corrugation of Gr film. (b) AFM image of Gr-AgNWs hybrid film in height contrast mode. (c) AFM image of Gr-AgNWs hybrid film in phase contrast mode.

controlled by spin coating cycles (see Supporting Information Figure S2). Note that the sheet resistance of monolayer Gr film is also shown in Figure 3a as a reference. It can be seen that the sheet resistances of AgNWs networks are lower than that of the Gr film and strongly dependent on the AgNWs density. More interestingly, the AgNWs network soldered by GO flakes shows lower sheet resistance than the AgNWs network in the case of the same AgNWs density. It is believed that the GO soldering

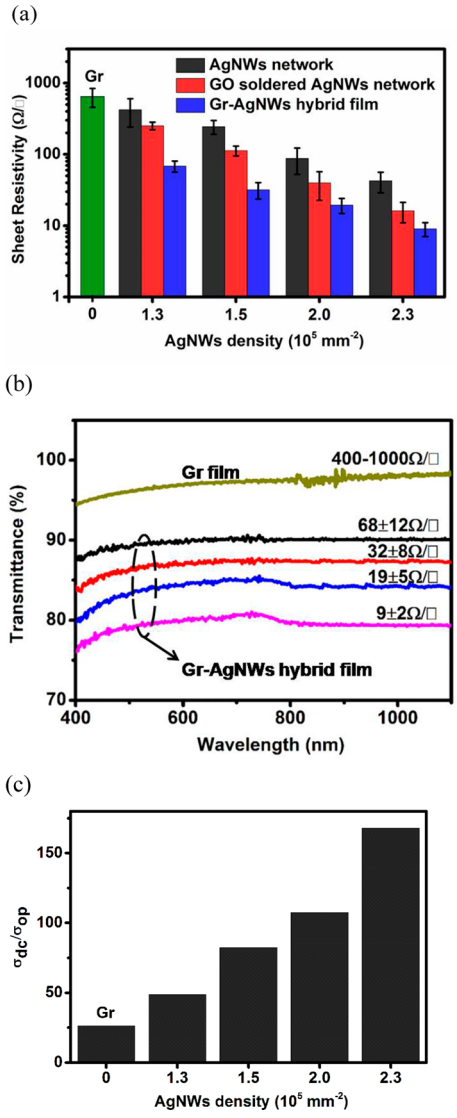

Figure 3. (a) Sheet resistances of Gr film, AgNWs networks, AgNWs networks soldered by GO flakes and Gr-AgNWs hybrid films as a function of AgNWs density. (b) Specula transmittance spectra of the Gr film and Gr-AgNWs hybrid films with different sheet resistance. (c) Values of σ_{dc}/σ_{op} for the Gr film and the Gr-AgNWs hybrid films with various AgNWs density.

significantly reduces the contact resistance between the AgNWs and thus enhances the conductivity of the AgNWs network. Among all kinds of the films, the Gr-AgNWs hybrid film has the lowest sheet resistance, as a result of both the AgNWs network and Gr film contributions. When the AgNWs density is 2.3 × 10^5 mm^{-2}, the sheet resistance of the Gr-AgNWs hybrid film can be as low as 9 Ω/□, quite suitable for solar cell fabrication. However, it is well-known that the dense AgNWs in the hybrid film usually result in the loss of light transmittance. Figure 3b compares the transmittance of Gr-AgNWs hybrid films with the Gr film. It can be seen that the transmittance of all the Gr-AgNWs hybrid films are indeed lower than the Gr film, due to the reflection of light by AgNWs. Meanwhile, the transmittance of Gr-AgNWs hybrid films is reduced from 90% to 78% (at the wavelength of 550 nm), when its sheet resistance decreases from 68 to 9 Ω/□. Lee et al.[17] and Chen et al.[18] have previously reported Gr-AgNWs hybrid films with sheet resistance of 33 Ω/□and 22 Ω/□, transparency of 94% and

DOI: 10.1021/am508211e
ACS Appl. Mater. Interfaces 2015, 7, 4135−4141

88% (at the wavelength of 550 nm), respectively. For comparison, our Gr-AgNWs hybrid film has relative lower sheet resistance (9 Ω/□) and transparency (78%) because the AgNWs used here have higher density and larger diameter.

Generally, the ratio of direct current and optical conductivity (σ_{dc}/σ_{op}) can be used as a figure-of-merit (MOF) to evaluate the optoelectronic performance of transparent conductors,[19] which can be expressed as

$$\frac{\sigma_{op}(\lambda)}{\sigma_{dc}} = \frac{2R_{Sh}}{273}\left(\frac{1}{T(\lambda)^2} - 1\right) \quad (1)$$

where T and R_{Sh} are the transmittance (quoted normally at λ = 550 nm) and the sheet resistance of the transparent conductor, respectively. The σ_{dc}/σ_{op} values of the Gr-AgNWs films with different AgNWs density and the Gr film can be obtained based eq 1, as shown in Figure 3c. Note that a high σ_{dc}/σ_{op} value means that the transparent conductor has superior optoelectronic property. It can be seen from Figure 3c that the σ_{dc}/σ_{op} values of Gr-AgNWs hybrid films, dependent on the AgNWs density, can reach to a maximal value of 168, which is much larger than that of the monolayer Gr film, about 26, and larger than the previous reported values of similar Gr-AgNWs hybrid films in the range 53−130.[20−22] The better ratio of direct current and optical conductivity of as-obtained Gr-AgNWs hybrid films originates from two aspects. On one hand, the electrical conductivity of AgNWs network can be significantly improved by GO soldering, see Figure 3a. On the other hand, the GO flakes that selectively wrap around the junctions of the AgNWs will not cause the obvious loss for the transparence of the Gr-AgNWs hybrid film, see Figure 1. Therefore, our Gr-AgNWs hybrid film has lager σ_{dc}/σ_{op} value and is more suitable for photovoltaic application.

Usually, the thermal stability of a transparent conductor is very important for its application in the solar cell fabrication. Figure 4, a and b, shows the scanning electron microscopy (SEM) micrographs of Gr-AgNWs hybrid films with and without GO soldering after 400 °C/1 h annealing in forming gas. It can be seen that the AgNWs network without GO soldering are broken extensively, which frequently takes place at the intersect points of network. However, the AgNWs network with GO soldering almost keep undamaged. It is believed that the heat accumulation tends to occur at the intersect points of AgNWs network, therefore easily resulting in the breakage of AgNWs at the intersect points. For the AgNWs network with GO soldering, the contact between the AgNWs and the Gr film may be optimized by the GO flakes, thus facilitating the heat transfer from the AgNWs network to the Gr film. Therefore, the AgNWs may be protected from breakage because the Gr film has excellent thermal conductivity.[23] Figure 4c shows the sheet resistances of the Gr-AgNWs hybrid films with and without GO soldering before and after 400 °C annealing for 1 h. It can be seen that the sheet resistance of the Gr-AgNWs hybrid films without GO soldering increases slightly after annealing. The increase of the sheet resistance is due to the breakage of AgNWs. However, even though the AgNWs were broken, they can still act as electric pathways bridging the graphene domains and bypass the high resistance gain boundaries of the Gr film.[24,25] Thus, the conductivity of the hybrid film is largely maintained. The sheet resistance of the Gr-AgNWs hybrid films with GO soldering even slightly decreases after annealing. It suggests that a post annealing can further optimize the conductivity of the Gr-AgNWs hybrid film with GO soldering.

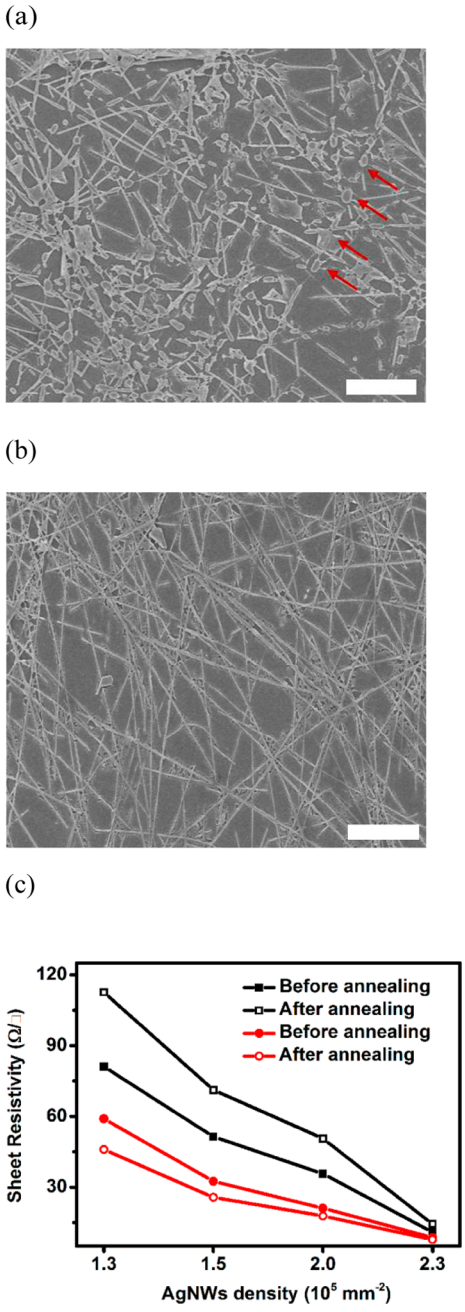

Figure 4. (a) SEM micrographs of Gr-AgNWs hybrid films without GO soldering after 400 °C/1 h annealing in forming gas. The arrows indicate the intersect points of AgNWs network where the AgNWs break. The scale bar is 5 μm. (b) SEM micrographs of Gr-AgNWs hybrid films with GO soldering after 400 °C/1 h annealing in forming gas. The scale bar is 5 μm. (c) Sheet resistances of Gr-AgNWs hybrid films with (circular points) and without (quadrate points) GO soldering before and after 400 °C/1 h annealing.

For solar cell fabrication, Gr-AgNWs hybrid film with σ_{dc}/σ_{op} value of 168 is utilized and the device-active areas are 16 mm^2 and 30 mm^2. The schematic structure and the SEM image of the Gr-AgNWs-Si solar cell in plan-view are shown by Figure 5a and c. The Gr film forms heterojunction with the *n*-Si, and the AgNWs network are buried under the Gr film as subelectrodes for carrier collection. For reference, the AgNWs-Si and Gr-Si

DOI: 10.1021/am508211e
ACS Appl. Mater. Interfaces 2015, 7, 4135−4141

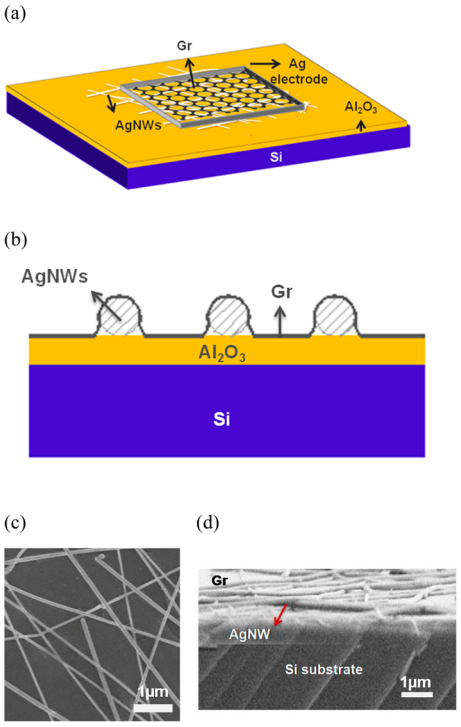

Figure 5. Schematic diagrams of Gr-AgNWs-Si solar cell in plan-view (a) and cross-section view (b). SEM images of Gr-AgNWs-Si solar cell in plain view (c) and cross-section view (d).

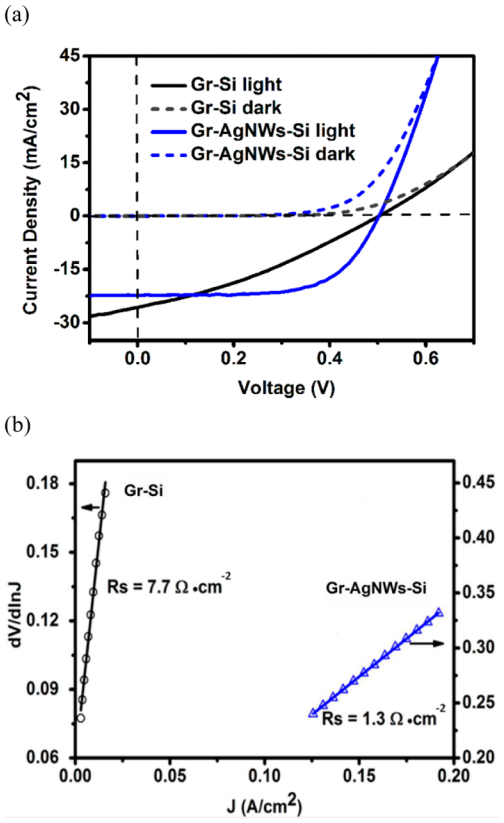

Figure 6. Performance characteristics of Gr-AgNWs-Si and Gr-Si solar cells: (a) current density−voltage (J−V) curves in dark and under illumination. (b) Series resistance (R_s) values extrapolated from dark $dV/(d \ln J)$ vs J curves.

solar cells are also fabricated. The current density−voltage (J−V) curves of the various solar cells in dark and under illumination circumstance are shown in Supporting Information Figure S4. Note that the rectification characteristic and the photovoltaic response of the AgNWs-Si device is much poorer than the Gr-Si devices, but those of Gr-Si and Gr-AgNWs-Si solar cells are quite close. Therefore, it is believed that, in such a structure, the Gr-Si contact plays a main role in the generation of interfacial barrier for carrier collection. To clarify the affect of AgNWs on the Gr film, field-effect transistor (FET) devices with Gr film and Gr-AgNWs hybrid film channels were fabricated and their drain−source current versus back-gate voltage (I_{ds}−V_g) curves were monitored, as shown in Supporting Information Figure S5. Note that the shift of the Dirac point voltage (V_{Dirac}) signals the chemical doping of the Gr film. The V_{Dirac} of FETs based on the Gr film and the Gr-AgNWs hybrid film are the same, suggesting that the AgNWs has no chemically doping effect on the Gr film. All these results lead us to believe that the main function of the AgNWs in the solar cell is to increase the electrical conductivity of the Gr film and facilitates the carrier transportation. The schematic structure and the SEM image of our Gr-AgNWs-Si solar cell in cross-section view are shown as Figure 5b and d. It should be stressed here that the advantage of the buried AgNWs under the Gr film is that the contact resistance between the Gr and AgNWs can be significantly reduced according to our experiences, which benefits for the carrier transportation between the Gr and AgNWs, and meanwhile, the buried AgNWs will be protected by the Gr film from oxidization, which is good for the device stability.[26]

Figure 6a compares the J−V curves of the Gr-Si and Gr-AgNWs-Si solar cells with a 16 mm^2 device-active area in dark and under illumination circumstance. Note that all the solar cells were subjected to a 400 °C/60 min for removing of the trapped H_2O and/or O_2 at the Gr-Si interface and optimizing the contact of the Gr film on Si.[27] Compared to the Gr-Si solar cell, the forward current of the Gr-AgNWs-Si solar cell in dark under positive bias gets significantly enhanced due to the introduction of the AgNWs network buried contacts. While under illumination, the open-circuit voltage of the Gr-AgNWs-Si solar cell is almost the same as that of the Gr-Si solar cell, which depends on the difference of work functions between Gr and Si. However, compared to the Gr-Si solar cell, the short circuit current (J_{SC}) of the Gr-AgNWs-Si solar cell becomes slightly smaller, due to the loss of transparence of the hybrid film. More importantly, the fill factor (FF) value of the Gr-AgNWs-Si solar cell is 0.63, much larger than that of the Gr-Si solar cell, 0.33. Figure 6b shows the series resistance (R_s) of the Gr-Si and Gr-AgNWs-Si solar cells with a 16 mm^2 device-active area. It can be seen that the series resistance of the Gr-AgNWs-Si solar cell is 1.3 Ω·cm^2, much smaller than that of the Gr-Si solar cell, 7.7 Ω·cm^2. Obviously, the improvement of FF value for the Gr-AgNWs-Si solar cell is attributed to the decrease of its series resistance, due to the application of buried AgNWs network. As a result, an efficiency of 7.18% can be obtained for the Gr-AgNWs-Si solar cell, which is much larger than that for the Gr-Si solar cell, about 4.31%. If further increasing the device area to 30 mm^2, it is found that the values of V_{OC} and J_{SC} for the Gr-AgNWs-Si solar cells almost keep constant, but the value of FF slightly decreases to 0.583, corresponding to R_s = 2.5 Ω·cm^2 and the efficiency is 6.69% (see Supporting Information Table S1). This result suggests that the resistive power loss effect of the Gr-AgNWs-Si solar cell must also take place with scaling-up its device-active area.

DOI: 10.1021/am508211e
ACS Appl. Mater. Interfaces 2015, 7, 4135−4141

Table 1. Comparison of the Stability of Our Gr-AgNWs-Si Solar Cell with Previously Reported Chemically Doped Gr-Si Solar Cell

solar cells	device-active area	original eff.	degraded eff.	degradation ratio	storing time	remarks
HNO_3 doped monolayer Gr-Si	9 mm^2	5.47%	2.96%	45.9%	8 days	ref 14
$AuCl_3$ doped four layer Gr-Si	9 mm^2	10.40%	9.65%	7.2%	7 days	ref 29
monolayer Gr-AgNWs-Si	16 mm^2	8.68%	8.42%	3.0%	7 days	this work

The utilization of antireflective film is generally a routine way to improving the absorption of light and therefore the J_{sc} values for solar cells. For our Gr-AgNWs-Si solar cells, the PMMA should be suitable as the antireflective film,[28] since its refractive index ($n_{PMMA} \approx 1.5$) is between Si ($n_{Si} \approx 4$) and air ($n_{air} \approx 1$). The optimized thickness of PMMA film is about 100 nm which could be controlled by spinning coating process. It is found that the efficiencies of Gr-AgNWs-Si solar cells with the device-active areas of 16 mm^2 and 30 mm^2 by spin-coating PMMA onto the surface can be improved to 8.68% and 8.37%, respectively. The improvements of solar cell efficiencies are mainly attributed to the increase of the J_{sc}, due to the antireflection of PMMA film.

The stability of solar cells is critical for their practical application in photovoltaics. In previous studies, the stability of volatile oxidants (such as HNO_3) and $AuCl_3$ doped Gr-Si solar cells are evaluated.[14,29] It is found that all of these chemically doped solar cells suffer efficiency degradation accompanying with the decreasing of V_{OC}, FF, and J_{SC} of the solar cell because of the subdued doping effect over time. Table 1 compares the efficiency degradation of our Gr-AgNWs-Si solar cells with that of chemically doped Gr-Si solar cells reported in the literatures. Note that our solar cells are stored in open air without encapsulation. The storing temperature and humidity are typically 25 °C and 60%, respectively. It is found that the efficiency of our Gr-AgNWs-Si solar cell loses only 3% of its original value (absolutely from 8.68% to 8.42%) after 7 days, much less than that of chemically doped devices, which is averagely 45% for HNO_3 doped device and 7% for $AuCl_3$ doped device. This result clearly indicates that the stability of our Gr-AgNWs-Si solar cells is much better than that of the chemically doped Gr/Si solar cells. Note that the efficiency of our Gr-AgNWs-Si solar cells degrades as a result of slightly reduction of FF, while the J_{SC} and V_{OC} keeping constant (see Supporting Information Figure S7). The reason for degradation needs more experiments to clarify.

CONCLUSIONS

In summary, we have developed a novel Gr-AgNWs hybrid film for photovoltaic application. The sheet resistance of such a hybrid film can be as low as 9Ω/□, with a σ_{dc}/σ_{op} ratio of 168. In the Gr-AgNWs-Si solar cells, the Gr-Si contact plays the main role in the formation of junction for carrier collection, and the AgNWs network acts as the buried subelectrodes for carrier transportation. An efficiency of 8.68% has been achieved for the Gr-AgNWs-Si solar cell with a device-active area of 16 mm^2. This value is the highest efficiency for the chemically doped-free Gr-Si solar cell reported by now. Furthermore, it is clarified that the Gr-AgNWs-Si solar cell has good stability, potential for practical application. These results point out a new route in developing large-scale, efficient, and stable Gr/Si solar cells.

ASSOCIATED CONTENT

Supporting Information

More detailed information regarding the SEM images of AgNWs networks fabricated by different spin coating cycles and their corresponding AgNWs density, the current density–voltage ($J-V$) curves of AgNWs-Si, Gr-Si, and Gr-AgNWs-Si devices in the dark and under illuminated, the current density–voltage ($J-V$) curves of Gr-Si solar cell optimized by annealing processes at varying temperatures, the device parameters of Gr-Si and Gr-AgNWs-Si solar cells studied in this work. This material is available free of charge via the Internet at http://pubs.acs.org.

AUTHOR INFORMATION

Corresponding Authors

*E-mail: yuxuegong@zju.edu.cn.
*E-mail: mseyang@zju.edu.cn.

Notes

The authors declare no competing financial interest.

ACKNOWLEDGMENTS

This work is supported by the National Natural Science Foundation of China (Nos. 61422404 and 61274057).

REFERENCES

(1) Novoselov, K. S.; Falko, V. I.; Colombo, L.; Gellert, P. R.; Schwab, M. G.; Kim, K. A Roadmap for Graphene. *Nature* **2012**, *490*, 192–200.
(2) Li, X.; Cai, W.; An, J.; Kim, S.; Nah, J.; Yang, D.; Piner, R.; Velamakanni, A.; Jung, I.; Tutuc, E.; Banerjee, S. K.; Colombo, L.; Ruoff, R. S. Large-Area Synthesis of High-Quality and Uniform Graphene Films on Copper Foils. *Science* **2009**, *324*, 1312–1314.
(3) Ye, Y.; Dai, L. Graphene-Based Schottky Junction Solar Cells. *J. Mater. Chem.* **2012**, *22*, 24224–24229.
(4) Lin, Y.; Li, X.; Xie, D.; Feng, T.; Chen, Y.; Song, R.; Tian, H.; Ren, T.; Zhong, M.; Wang, K.; Zhu, H. Graphene/Semiconductor Heterojunction Solar Cells with Modulated Antireflection and Graphene Work Function. *Energy Environ. Sci.* **2013**, *6*, 108–115.
(5) Li, X.; Zhu, H.; Wang, K.; Cao, A.; Wei, J.; Li, C.; Jia, Y.; Li, Z.; Li, X.; Wu, D. Graphene-on-Silicon Schottky Junction Solar Cells. *Adv. Mater.* **2010**, *22*, 2743–2748.
(6) Zhang, X. Z.; Xie, C.; Jie, J. S.; Zhang, X. W.; Wu, Y. M.; Zhang, W. J. High-Efficiency Graphene/Si Nanoarray Schottky Junction Solar Cells via Surface Modification and Graphene Doping. *J. Mater. Chem. A* **2013**, *1*, 6593–6601.
(7) Xie, C.; Zhang, X. Z.; Wu, Y. W.; Zhang, X. J.; Zhang, X. W.; Wang, Y.; Zhang, W. J.; Gao, P.; Han, Y. Y.; Jie, J. S. Surface Passivation and Band Engineering: A Way Toward High Efficiency Graphene–Planar Si Solar Cells. *J. Mater. Chem. A* **2013**, *1*, 8567–8574.
(8) Yang, L. F.; Yu, X. G.; Xu, M. S.; Chen, H. Z.; Yang, D. R. Interface Engineering for Efficient and Stable Chemical-Doping-Free Graphene-on-Silicon Solar Cells by Introducing a Graphene Oxide Interlayer. *J. Mater. Chem. A* **2014**, *2*, 16877–16883.
(9) An, X.; Liu, F.; Kar, S. Optimizing Performance Parameters of Graphene–Silicon and Thin Transparent Graphite–Silicon Heterojunction Solar Cells. *Carbon* **2013**, *57*, 329–337.

DOI: 10.1021/am508211e
ACS Appl. Mater. Interfaces 2015, 7, 4135–4141

(10) Nair, R. R.; Blake, P.; Grigorenko, A. N.; Novoselov, K. S.; Booth, T. J.; Stauber, T.; Peres, N. M. R.; Geim, A. K. Fine Structure Constant Defines Visual Transparency of Graphene. *Science* **2008**, *320*, 1308−1308.
(11) Bae, S.; Kim, H.; Lee, Y.; Xu, X.; Park, J.-S.; Zheng, Y.; Balakrishnan, J.; Lei, T.; Ri Kim, H.; Song, Y. I.; Kim, Y.-J.; Kim, K. S.; Ozyilmaz, B.; Ahn, J.-H.; Hong, B. H.; Iijima, S. Roll-to-Roll Production of 30-Inch Graphene Films for Transparent Electrodes. *Nat. Nanotechnol.* **2010**, *5*, 574−578.
(12) Miao, X.; Tongay, S.; Petterson, M. K.; Berke, K.; Rinzler, A. G.; Appleton, B. R.; Hebard, A. F. High Efficiency Graphene Solar Cells by Chemical Doping. *Nano Lett.* **2012**, *12*, 2745−2750.
(13) Shi, E.; Li, H.; Yang, L.; Zhang, L.; Li, Z.; Li, P.; Shang, Y.; Wu, S.; Li, X.; Wei, J.; Wang, K.; Zhu, H.; Wu, D.; Fang, Y.; Cao, A. Colloidal Antireflection Coating Improves Graphene−Silicon Solar Cells. *Nano Lett.* **2013**, *13*, 1776−1781.
(14) Cui, T.; Lv, R.; Huang, Z.-H.; Chen, S.; Zhang, Z.; Gan, X.; Jia, Y.; Li, X.; Wang, K.; Wu, D.; Kang, F. Enhanced Efficiency of Graphene/Silicon Heterojunction Solar Cells by Molecular Doping. *J. Mater. Chem. A* **2013**, *1*, 5736−5740.
(15) Li, X. S.; Zhu, Y.; Cai, W.; Borysiak, M.; Han, B.; Chen, D.; Piner, R. D.; Colombo, L.; Ruoff, R. S. Transfer of Large-Area Graphene Films for High-Performance Transparent Conductive Electrodes. *Nano Lett.* **2009**, *12*, 4359−4363.
(16) Liang, J. J.; Li, L.; Tong, K.; Ren, Z.; Hu, W.; Niu, X. F.; Chen, Y. S.; Pei, Q. B. Silver Nanowire Percolation Network Soldered with Graphene Oxide at Room Temperature and Its Application for Fully Stretchable Polymer Light Emitting Diodes. *ACS Nano* **2014**, *8*, 1590−1600.
(17) Lee, M.; Lee, K.; Kim, S.; Lee, Y. H.; Park, J.; Choi, K. H.; Kim, H. K.; Kim, D. G.; Lee, D. Y.; Nam, S. W.; Park, J. U. High-Performance, Transparent, and Stretchable Electrodes Using Graphene−Metal Nanowire Hybrid Structures. *Nano Lett.* **2013**, *13*, 2814−2821.
(18) Chen, R.; Das, S. R.; Jeong, C.; Khan, M. R.; Janes, D. B.; Alam, M. A. Co-Percolating Graphene-Wrapped Silver Nanowire Network for High Performance, Highly Stable, Transparent Conducting Electrodes. *Adv. Funct. Mater.* **2013**, *23*, 5150−5158.
(19) Ellmer, K. Past Achievements and Future Challenges in the Development of Optically Transparent Electrodes. *Nat. Photonics* **2012**, *6*, 809−817.
(20) Liu, Y.; Chang, Q.; Huang, L. Transparent, Flexible Conducting Graphene Hybrid Films with a Subpercolating Network of Silver Nanowires. *J. Mater. Chem. C* **2013**, *1*, 2970−2974.
(21) Chen, T. L.; Mkhitaryan, V.; Pruneri, V. Hybrid Transparent Conductive Film on Flexible Glass Formed by Hot-Pressing Graphene on a Silver Nanowire Mesh. *ACS Appl. Mater. Interfaces* **2013**, *5*, 11756−11761.
(22) Iskandar, N.; Kholmanov, C. W. M.; Aliev, A. E.; Li, H. F.; Zhang, B.; Suk, J. W.; Zhang, L. L.; Peng, E.; Mousavi, S. H.; Khanikaev, A. B.; Piner; Shvets, R. G.; Ruoff, R. S. Improved Electrical Conductivity of Graphene Films Integrated with Metal Nanowires. *Nano Lett.* **2012**, *12*, 5679−5683.
(23) Harrington, M. J.; Masic, A.; Andersen, N. H.; Waite, J. H.; Fratzl, P. Two-Dimensional Phonon Transport in Supported Graphene. *Science.* **2010**, *328*, 213−216.
(24) Jeong, C. W.; Nair, P.; Khan, M.; Lundstrom, M.; Alam, M. A. Prospects for Nanowire-Doped Polycrystalline Graphene Films for Ultratransparent, Highly Conductive Electrodes. *Nano Lett.* **2011**, *11*, 5020−5025.
(25) Choi, H. O.; Kim, D. W.; Kim, S. J.; Yang, S. B.; Jung, H. T. Role of 1D Metallic Nanowires in Polydomain Graphene for Highly Transparent Conducting Films. *Adv. Mater.* **2014**, *26*, 4575−4581.
(26) Lee, D.; Lee, H.; Ahn, Y.; Jeong, Y.; Lee, D.-Y.; Lee, Y. Highly Stable and Flexible Silver Nanowire−Graphene Hybrid Transparent Conducting Electrodes for Emerging Optoelectronic Devices. *Nanoscale* **2013**, *5*, 7750−7755.
(27) Kim, D. J.; Park, N. W.; Lee, W. Y.; Sim, Y.; Kim, K. S.; Seongb, M.; Koh, J. H.; Hong, C. H.; Lee, S. K. Effect of Annealing of Graphene Layer on Electrical Transport and Degradation of Au/Graphene/N-type Silicon Schottky Diodes. *J. Alloys Compd.* **2014**, *612*, 265−272.
(28) Li, R.; Di, J.; Yong, Z.; Sun, B.; Li, Q. Polymethylmethacrylate Coating on Aligned Carbon Nanotube−Silicon Solar Cells for Performance Improvement. *J. Mater. Chem. A* **2014**, *2*, 4140−4143.
(29) Xie, C.; Zhang, X.; Ruan, K.; Shao, Z.; Dhaliwal, S. S.; Wang, L.; Zhang, Q.; Zhang, X.; Jie, J. High-Efficiency, Air Stable Graphene/Si Micro-Hole Array Schottky Junction Solar Cells. *J. Mater. Chem. A* **2013**, *1*, 15348−15354.

DOI: 10.1021/am508211e
ACS Appl. Mater. Interfaces 2015, 7, 4135−4141